Chemical Science

ROYAL SOCIETY OF CHEMISTRY

EDGE ARTICLE

View Article Online
View Journal

Cite this: DOI: 10.1039/d5sc07083j

All publication charges for this article have been paid for by the Royal Society of Chemistry

Thermal decomposition behavior and sustainable recycling of flexible perovskite solar modules

Xiaoyu Shi, Yangyang Liu, Tianxiao Liu, Siwei Luo, Feifei Wang and Shangshang Chen *

The environmental implications of all photovoltaic (PV) technologies should be rigorously assessed throughout their entire lifecycle. Perovskite PVs have emerged as a transformative innovation, challenging the dominance of conventional silicon PVs, with numerous companies now commercializing this promising technology. While efforts to enhance the efficiency and longevity of perovskite PVs are crucial, it is equally important to develop sustainable and cost-effective methods for disposing of waste perovskite solar panels, especially given their significant content of water-soluble lead ions. In this study, we explore the feasibility of employing incineration to process degraded flexible perovskite solar modules. We analyze the decomposition byproducts and their potential environmental impacts. By implementing careful management of hazardous decomposition products, we demonstrate that incineration can serve as a sustainable and economical solution for the disposal of waste perovskite solar modules, offering valuable insights for the future handling of these materials.

Received 14th September 2025
Accepted 8th January 2026

DOI: 10.1039/d5sc07083j

rsc.li/chemical-science

1 Introduction

Since the 1990s, solar photovoltaic (PV) power generation has experienced robust and steady growth with an annual rate of 37%, positioning solar energy as the fastest-growing renewable energy source.[1–3] More intuitively, the cumulative PV installed capacity, which stood at a mere 1.28 GW in 2000, surged to a cumulative PV capacity of 709.67 GW by 2020.[4] Meanwhile, the emergence of new thin-film PV technologies has also significantly contributed to the development of solar PVs, particularly perovskite PVs that exhibit advantages including low-cost manufacturing, light weight, and mechanical flexibility.[5,6] Compared to rigid and heavy silicon PVs, perovskite PVs have huge application potential in building-integrated, foldable, and flexible PVs.

As the scale of PV power installation continues to expand, the environmental implications of these PV panels must be rigorously assessed throughout their entire lifecycle. Global PV module waste is expected to surge to 60–78 million tons (equivalent to 630 GW) by 2050.[7] The existing PV waste management strategies, which mainly focus on crystalline silicon modules, include landfilling and recycling.[8,9] Among them, recycling, which aligns with the principles of environmental sustainability and resource recovery, stands as the most extensively researched disposal method. The recycling process for crystalline silicon modules involves physical separation, chemical treatment, and heat treatment, aiming to efficiently recover valuable materials such as silicon, Ag, and Cu while minimizing environmental pollution.[10] However, the recycling approach faces multiple challenges. The first is the environmental challenge, which includes the release of extremely harmful gases, such as hydrofluoric acid, during chemical treatments, as well as the dust and noise generated during physical processes like high-pressure crushing.[11–13] The second challenge is economic feasibility because the cost of establishing and operating recycling infrastructures is relatively high.[7,14] Additionally, the economic viability of recycling is also constrained by the limited quantity and overall value of recoverable materials.[15–18] The related studies have indicated that the recycled products of crystalline silicon modules are mainly composed of 68% glass and 15% base Al metal.[9,19] The low value of these materials, combined with the high costs of recycling and disposal, results in a lack of economic sustainability for this recycling method.

Emerging as a transformative innovation challenging conventional silicon PVs, perovskite PV technology has attracted hundreds of industrial players pursuing its commercialization.[20,21] While ongoing research focuses on enhancing device efficiency and operational stability, equal emphasis must be placed on developing sustainable and economically viable disposal methods for end-of-life perovskite modules, particularly given their substantial environmental risk from high concentrations of water-soluble lead compounds.[22–24] Current recycling strategies primarily target the recovery of conductive substrates and PbI_2 precursors, yet critical challenges persist: the economic feasibility of PbI_2 reprocessing remains unproven

State Key Laboratory of Coordination Chemistry, MOE Key Laboratory of High-Performance Polymer Materials & Technology, School of Chemistry, Nanjing University, Nanjing, Jiangsu 210023, P. R. China. E-mail: schen@nju.edu.cn

(particularly as large amounts of solvents are involved), while flexible conductive substrates often suffer irreversible degradation from mechanical stress and environmental exposure during operational lifespan. These limitations underscore the urgent need for alternative disposal solutions to ensure the sustainable development of perovskite PVs.

Traditional landfill disposal of household waste presents unacceptable environmental hazards due to potential pollution to soil and groundwater systems.[25–28] Modern waste management practice demonstrates that advanced incineration technologies, when equipped with proper emission control systems and ash treatment protocols, can achieve both economic viability and environmental safety.[29,30] Drawing inspiration from these developments, this study systematically investigates the thermal decomposition pathways of degraded flexible perovskite solar modules. Through comprehensive analysis of incineration byproducts (including solid residues and gaseous emissions), we characterize the complete incineration profile and propose optimized post-treatment protocols for resultant materials, providing important guidance for the post-treatment of degraded perovskite modules. Our findings demonstrate that controlled incineration, when integrated with appropriate flue gas purification and ash stabilization techniques, presents a promising dual solution addressing both economic constraints and environmental concerns in perovskite PV waste management.

2 Results and discussion

2.1. Module incineration and ash analysis

The complete thermal degradation profile and analytical results are systematically presented in Fig. 1. For this investigation, we employed a representative flexible perovskite module architecture of polyethylene terephthalate (PET)/indium tin oxide (ITO)/poly[bis(4-phenyl)(2,4,6-trimethylphenyl)amine] (PTAA)/perovskite/C_{60}/bathocuproine (BCP)/Cu. The perovskite active layer comprised $Cs_{0.1}FA_{0.9}PbI_3$ (FA^+: formamidinium) composition, widely adopted in commercial module fabrication due to its high efficiency and thermal stability.[31,32] The pristine perovskite modules were able to realize a high power conversion efficiency (PCE) of 15.6% at an aperture area of 59.3 cm^2, with an open-circuit voltage (V_{OC}) of 16.2 V (1.16 V for each sub-cell), a short-circuit current (I_{SC}) of 82.4 mA, and a fill factor (FF) of 0.691 (Fig. S1). Then the unencapsulated module was put under light soaking to accelerate the natural degradation. To simulate real-world disposal conditions while ensuring complete incineration, modules were subjected to controlled incineration in a chamber under continuous air supply. Post-incineration ash residues were first analyzed *via* X-ray photoelectron spectroscopy (XPS) to determine elemental composition, chemical speciation, and potential lead-containing byproducts. Note that the encapsulants like polyolefin elastomer (POE) or polyisobutylene (PIB) were not involved in this study, as their incineration products have been well studied previously.[33,34]

As shown in Fig. 2a, the C 1s spectrum of the ash displays three binding energies at 284.5, 285.6, and 288.9 eV, which can be assigned to C–C/C–H, C–N, and C===O, respectively. The characteristic peak observed at 400.0 eV in the N 1s XPS spectrum (Fig. 2b) provides additional evidence for the presence of C–N bonds within the obtained ash,[35] which could potentially originate from residual FA^+ or insufficiently combusted BCP or PTAA compounds. The Pb 4f peak at 138.5 eV (Fig. 2c) is well assigned to that of PbI_2 (138.5 eV),[36] indicating a large amount of PbI_2 remaining in the ash after incineration. In addition, the presence of a characteristic shoulder at 138.9 eV suggested the formation of a complex mixture rather than pure PbI_2, potentially comprising various oxide phases and possibly carbonates. This can also be verified by the peak of corresponding β-PbO and/or $PbCO_3$ with a binding energy of 531.7 eV in the O 1s XPS

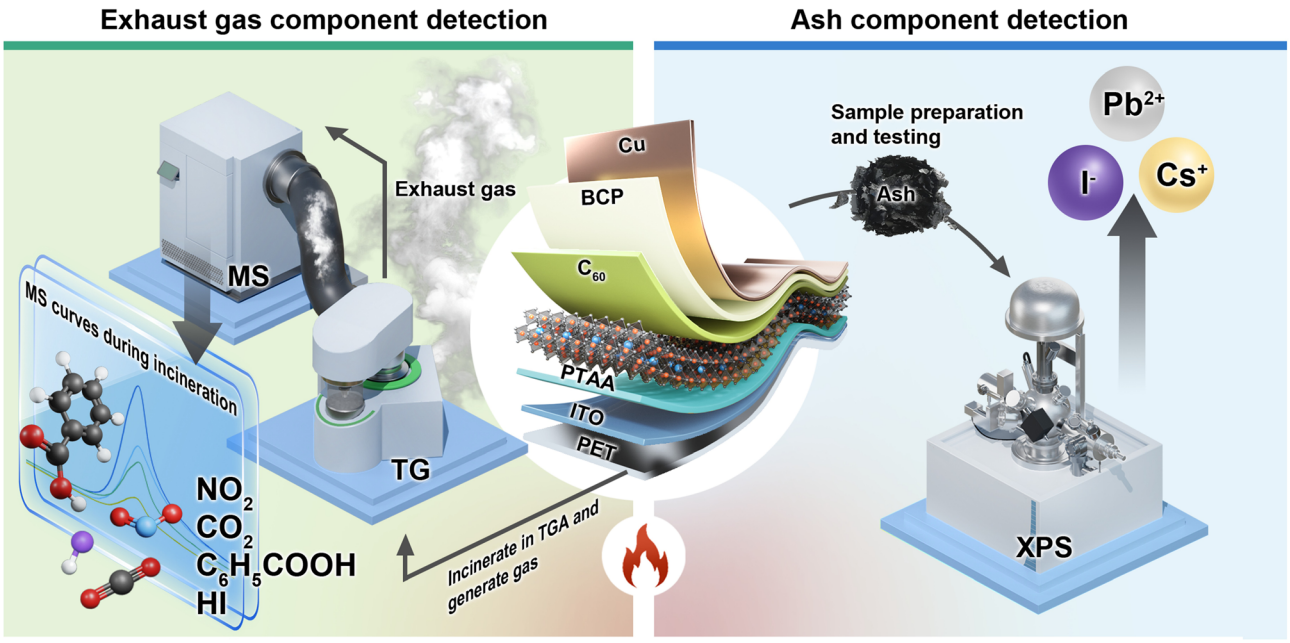

Fig. 1 Schematic illustration of the incineration product analysis of degraded flexible perovskite solar modules.

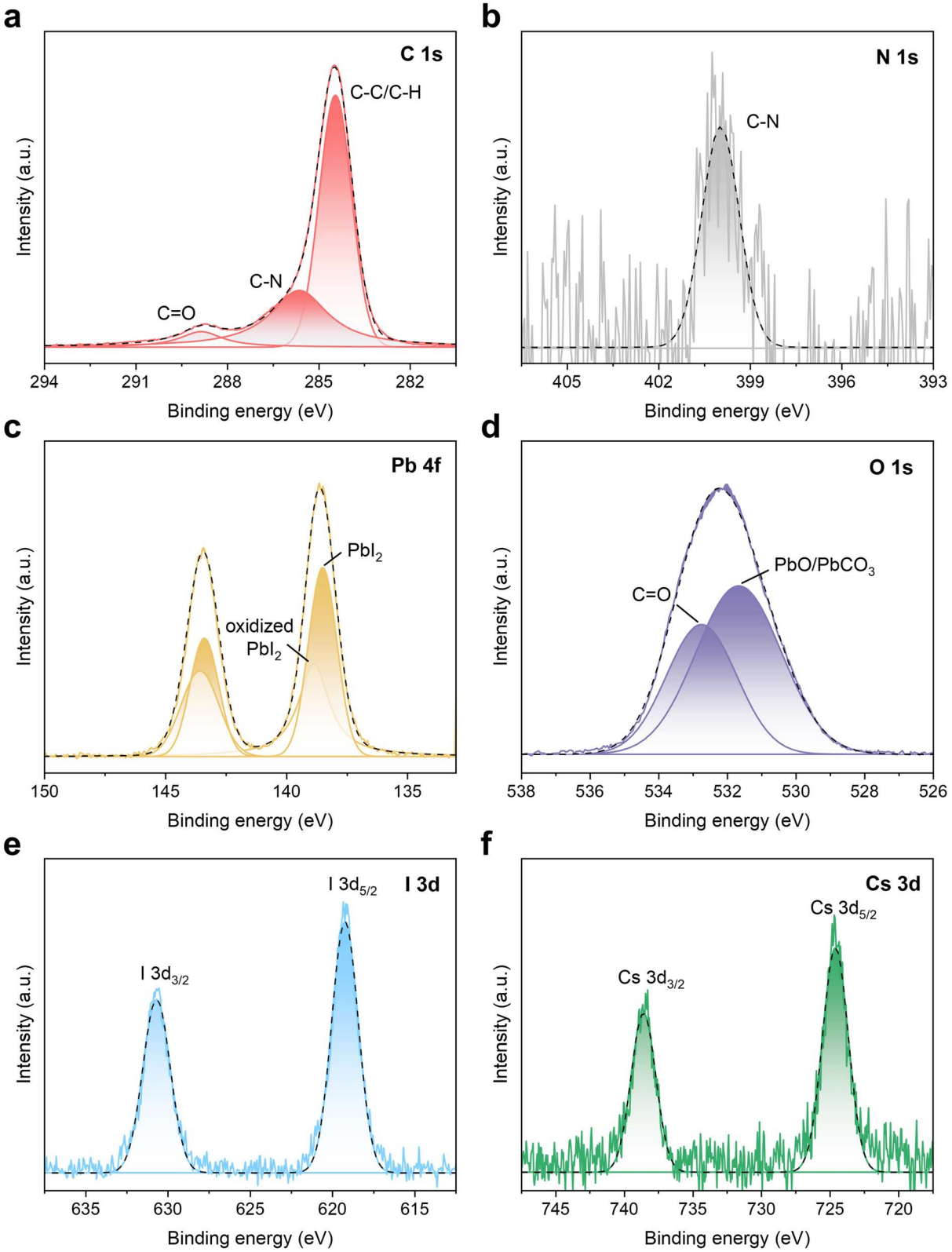

Fig. 2 XPS analysis of the ash obtained from incineration: (a) C 1s, (b) N 1s, (c) Pb 4f, (d) O 1s, (e) I 3d, and (f) Cs 3d.

spectrum (see Fig. 2c and d, respectively).[37,38] Furthermore, the XPS spectra of I 3d and Cs 3d are presented in Fig. 2e and f. The characteristic peaks of I $3d_{5/2}$ and I $3d_{3/2}$ are identified at binding energies of 619.2 eV and 630.7 eV, while Cs $3d_{5/2}$ and Cs $3d_{3/2}$ peaks are observed at 724.6 eV and 738.6 eV, respectively.[39,40] These spectral features are consistent with the spectra

of I^- and Cs^+ in the perovskite structure. Overall, following the incineration of waste flexible modules, the predominant chemical states of key elements in the residual solid ash are identified as Pb^{2+} (primarily existing in PbI_2, PbO, and $PbCO_3$ compounds), along with Cs^+ and I^-. The ash residue can be further recycled to reproduce the PbI_2 precursor.

Besides the elements present in the perovskite light-absorbing layer, we also analyzed the chemical states of electrode materials after incineration, including ITO and Cu. Similarly, XPS analysis was performed on key metallic elements including In, Sn, and Cu, within these incineration products (Fig. 3a–c). The results reveal that the In element primarily exists as In_2O_3, evidenced by the corresponding binding energy of 445.1 eV.[41,42] Furthermore, the binding energy of Sn $3d_{5/2}$ located at 487.0 eV indicates the presence of Sn^{4+}, thereby confirming the possibility of the existence of SnO_2.[43] As presented in Fig. 3c, the Cu $2p_{3/2}$ spectrum exhibits two distinct peaks located at 932.8 and 934.0 eV, respectively, demonstrating that the Cu element exists in the form of Cu^+ and Cu^{2+} oxidation states within the incineration products of burned waste flexible perovskite modules.[44,45] To verify the above conclusion, the PET-ITO flexible substrate coated with a 130-nm-thick Cu layer was subjected to identical incineration. Subsequently, as shown in Fig. 3d, X-ray diffraction (XRD) analysis was performed on the resulting residue. The diffraction pattern closely matched the standard card for In_2O_3 (PDF#06-0416), strongly supporting the presence of crystalline In_2O_3 in the pyrolyzed residue, consistent with the XPS results. However, it is noteworthy that no characteristic diffraction peaks associated with Cu were detected in the XRD pattern. Given that XPS identified Cu and its oxidation states, we infer that this absence is most likely attributable to the relatively low Cu content in the sample or its existence in an amorphous form, resulting in a diffraction signal below the XRD detection limit or indistinguishable from the background. Collectively, the above results elucidate the primary chemical speciation of key metallic elements within the pyrolyzed residue of electrodes (ITO/Cu) from waste flexible PV modules: In element predominantly exists as crystalline In_2O_3;

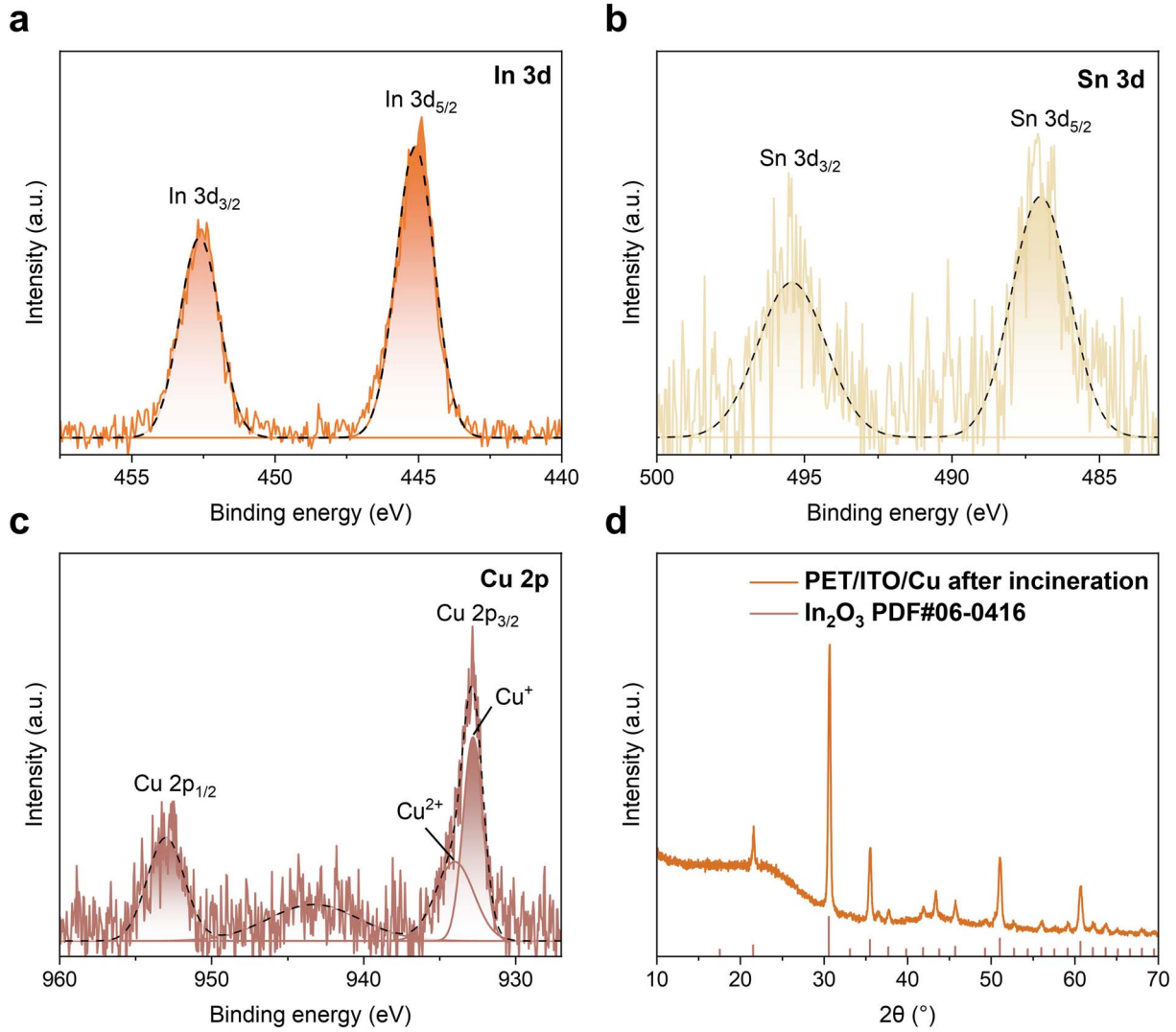

Fig. 3 XPS analysis of the ash obtained from incineration: (a) In 3d, (b) Sn 3d, and (c) Cu 2p. (d) XRD pattern of the ash after incineration of the PET/ITO/Cu sample.

Sn is stabilized in the Sn^{4+} oxidation state within the SnO_2 matrix; and Cu co-exists in both Cu^{+} and Cu^{2+} oxidation states. This result directly confirms the elemental transformation pathways of electrode materials during incineration.

2.2. Thermal decomposition and exhaust analysis

To systematically investigate the thermal decomposition behavior of the waste module, gas analysis was then conducted using TG-MS at a heating rate of 10 °C min^{-1} in ambient air. The experiment was conducted using a combination of TG analyzer and MS technology to enable real-time monitoring of mass loss dynamics and formation of gaseous species. As shown in Fig. 4a, TG curves reveal four distinct thermal decomposition stages. The flexible module demonstrates remarkable thermal stability below 300 °C with negligible mass loss (1.5%), indicating that the module has little moisture content and few low-temperature volatile components. Within the temperature range of 300–465 °C, the sample undergoes significant thermal decomposition, resulting in a mass loss of 89%. Furthermore, by analyzing the derivative TG curve, a prominent peak at 438 °C can be observed, signifying the maximum thermal decomposition rate of the sample at this

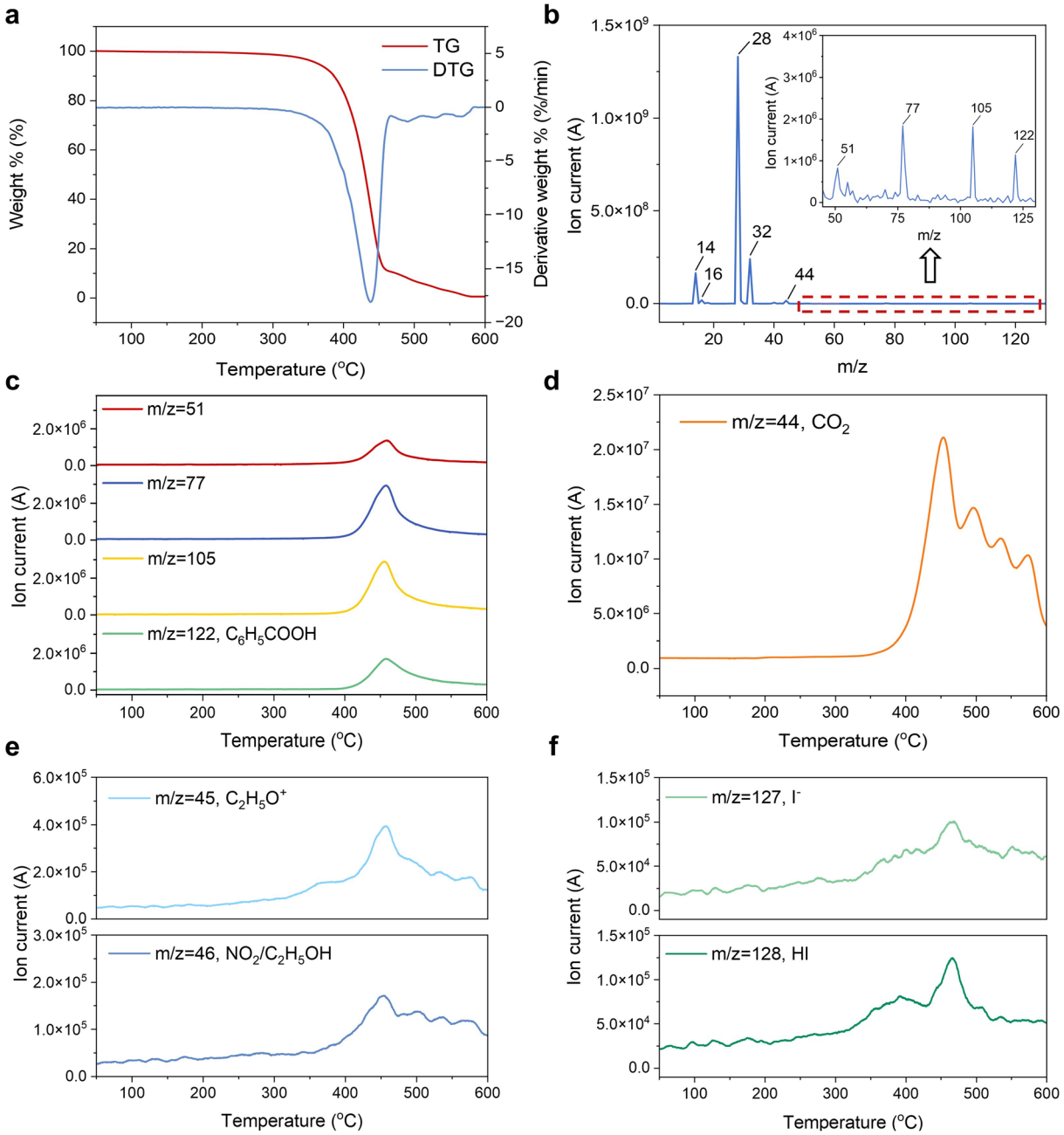

Fig. 4 TG-MS analysis of the exhaust during incineration. (a) TG-DTG curve of incineration of waste flexible module at a heating rate of 10 °C min^{-1}. (b) MS spectral diagram of thermal decomposition products at 438 °C (the inset is an enlarged image in the *m*/*z* range of 45 to 130). (c–f) The ion current intensity of the major gaseous fragments released from thermal decomposition products in ambient air.

temperature. This intensive mass loss is mainly attributed to the decomposition and volatilization of organic macromolecular substances into small molecular substances.[46] In the temperature range of 465–600 °C, there are three small peaks in the derivative thermogravimetry (DTG) curve, corresponding to 491, 530, and 567 °C, respectively. This stage is mainly for the formation of carbon ash and decomposition of some inorganic substances.[47] Beyond 600 °C, the rate of weight loss stabilizes, indicating that the thermal decomposition of the material is nearly complete. Since the thermal decomposition behavior of C_{60} has been extensively studied previously,[48–50] we did not investigate this point in the present work.

To systematically investigate the thermal decomposition behavior of the waste module, gas analysis was then conducted using TG-MS. Fig. 4b presents the mass spectrum acquired at the DTG peak temperature (438 °C), revealing predominant characteristic ions corresponding to N^+ (the mass/charge ratio (m/z) = 14), O^+ (m/z = 16), N_2 (m/z = 28), O_2 (m/z = 32), and CO_2 (m/z = 44).[47] Furthermore, the inset diagram in Fig. 4b presents an enlarged view of the m/z 45–130 region. The observed characteristic peaks at m/z = 51, 77, and 105 exhibit a strong correlation with the standard characteristic peaks of the benzoic acid molecule (C_6H_5COOH). Additionally, the molecular ion peak at m/z = 122 corresponds to the C_6H_5COOH from PET substrate, providing definitive evidence for its identification.[51,52] Fig. 4c–f show the ionic current curves of typical gas fragments with temperature, and the signal intensity is positively correlated with the concentration of the corresponding substance. Specifically, the ion current curve of m/z = 44 (CO_2) with temperature (Fig. 4d) exhibits multi-stage release characteristics: an initial emission peak at 453 °C followed by secondary peaks at 497, 536, and 574 °C, which correspond well with the peak points of the weight loss rate on the DTG curve. This multi-step release mechanism is due to the differential thermal stability of the multilayer structure of the device. The primary CO_2 arises from the deacetylation reaction of ethylene-vinyl acetate, the incineration product of PET, while subsequent emissions originate from further cleavage of remaining organic substances and oxidation of organic molecules such as PTAA, BCP, and C_{60} at elevated temperatures.[53] Notably, weak signals of the ion current are detected near a temperature of 453 °C (Fig. 4e), which correspond to the thermal decomposition products m/z = 45 ($C_2H_5O^+$) and 46 (NO_2). The generation of NO_2 is primarily due to the oxidation of the PTAA and BCP layers in the components, as well as the FA^+ in the active layer. In addition, trace signals of m/z = 127 and 128 are detected near 467 °C (Fig. 4f), which correspond to ion peaks of I^- and HI, respectively, which are obtained by thermal decomposition of the perovskite layer. The low ionic current values of these peaks indicate that halogen ion products from decomposition of the perovskite active layer account for a very low proportion in the tail gas.

TG analysis indicates that the incineration of the waste flexible module primarily occurs between 300 and 465 °C, with complete incineration occurring around 600 °C. TG-MS analysis reveals that the principal gaseous products generated during the incineration of waste flexible modules include CO_2, NO_2, C_2H_5OH, C_6H_5COOH, and HI. Notably, I_2 was hypothesized as a potential major decomposition product, but its detection proved challenging through conventional MS due to its solidification inside the channel before reaching the detector.

To verify whether iodine vapor is produced during the incineration of the waste module, we further set up a simple detection test as shown in Fig. S2a. First, we cut the discarded flexible module into small pieces and put them in a crucible, which was then positioned inside a stainless-steel pipe (painted as a glass tube in the schematic diagram for clarity). The polytetrafluoroethylene piston T-shaped three-way joint can be connected to both the balloon and the stainless-steel pipe separately by using polyurethane (PU) tubes. The exhaust outlet was connected *via* the PU tubing to a conical flask containing a starch indicator. Before starting the heating, the T-valve was opened to introduce O_2 from the balloon into the system. Then, the bottom of the stainless-steel pipe was continuously heated using a butane air gun. After about 2 minutes, the starch indicator in the conical flask visibly changed from white to purple, as shown in Fig. S2b and S2c, indicating that iodine vapor was indeed produced during the incineration process of the waste module, thus confirming our hypothesis.

2.3. Sustainable management and recycling

Through systematic analysis of incineration byproducts, we demonstrate that thermal treatment can serve as a sustainable disposal method for waste flexible perovskite modules, provided that exhaust gases and residual ash are properly managed like the incineration of household waste. The acidic exhaust gases can be effectively treated using established alkaline scrubbing systems containing $NH_3 \cdot H_2O$ or $Ca(OH)_2$ – a technology already widely implemented in municipal solid waste incineration facilities.

The resulting ash, containing valuable rare metals (In) and toxic heavy metals (Pb), requires centralized processing with particular attention to preventing Pb contamination. While the economic feasibility of metal recovery remains a consideration, we propose a comprehensive recycling protocol for incineration residues from perovskite modules (Fig. 5). Our approach addresses two critical challenges simultaneously: (1) safe containment of hazardous Pb and (2) recovery of strategically important elements (In and Cu). Notably, the combustion process generates primarily acidic off-gases, which can be efficiently neutralized through absorption in alkaline solutions (*e.g.*, aqueous ammonia). This integrated treatment strategy not only ensures environmental safety but also enables resource recovery from end-of-life PV devices. For the most metal ions in the ash, they can first be treated with an acidic solution (such as HNO_3) to dissolve the components to form soluble Pb^{2+} and Cu^{2+}, which can subsequently be precipitated as PbI_2 ($K_{sp} = 1.39 \times 10^{-8}$) and CuI ($K_{sp} = 1.1 \times 10^{-12}$) by adding KI. Since the solubility of PbI_2 increases significantly above 80 °C, a temperature gradient method can be used to separate PbI_2 from CuI. By heating, most of the PbI_2 dissolves, and the CuI precipitate is filtered off while still hot. The solution is then cooled to 0–4 °C to obtain PbI_2 precipitate.[54] As for In_2O_3, it can first be dissolved in an acid solution to form $InCl_3$. Then, ammonia water is added to it to generate $In(OH)_3$. Finally, a dehydration reaction

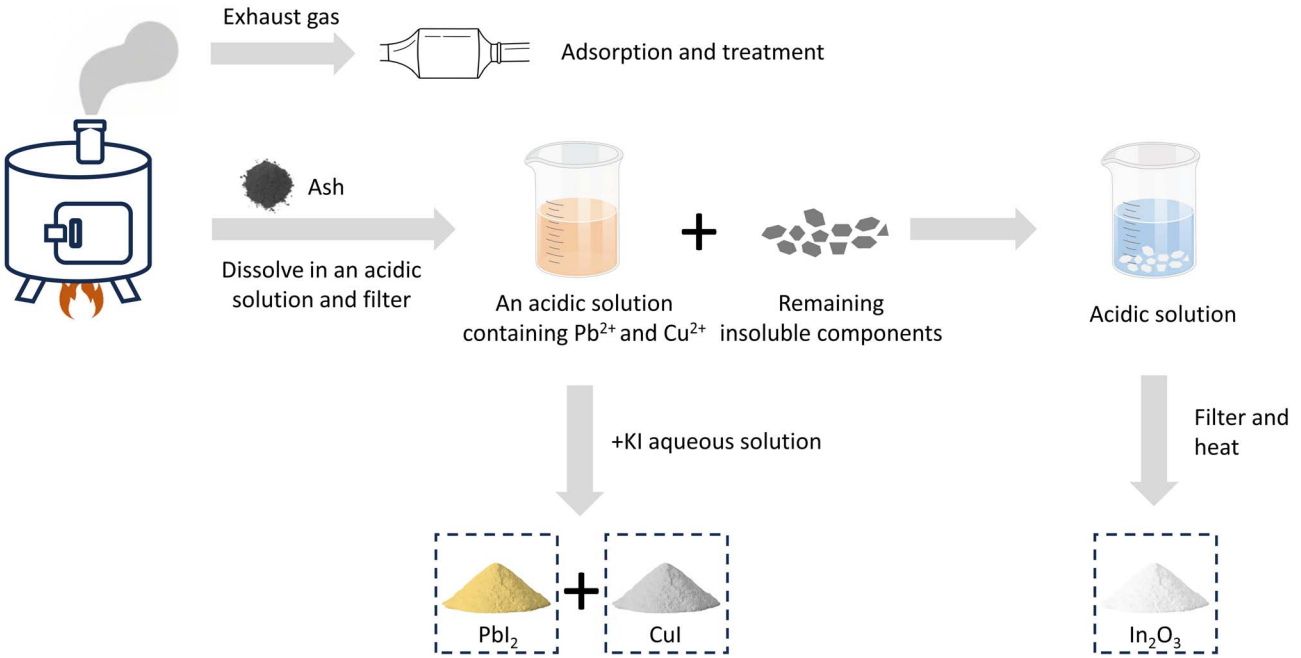

Fig. 5 Schematic illustration of a proposed management strategy for incineration products of degraded flexible perovskite modules.

at high temperature is carried out to produce pure In_2O_3. A lab-scale trial was carried out to verify the feasibility of the proposed recycling scheme. The specific experimental procedures and the analysis of the resulting products are presented in the SI.

Building upon the preceding analysis, the integrated incineration process, synergistically coupled with the hydrometallurgical recovery pathway outlined earlier, presents a viable and promising technological solution for the future large-scale treatment of waste flexible perovskite PV modules. This combined approach offers a tripartite advantage: first, it effectively decomposes organic constituents such as the polymer substrate and organic charge transport layers; second, it concentrates valuable (*e.g.*, In and Cu) and potentially toxic metals (notably Pb) within the residual ash; and third, it enables the stabilization of hazardous Pb while facilitating the efficient, sequential resource recovery of critical elements like In, Cu, and I through tailored wet-chemical techniques. It is worth mentioning that all chemicals in this process are aqueous solutions, and no organic solvents (*e.g.*, DMF or alcohols) are involved. Consequently, this integrated strategy significantly mitigates environmental hazards associated with landfilling or improper disposal, while simultaneously ensuring economic feasibility through the recuperation of valuable materials, thereby offering a holistic and sustainable end-of-life management solution.

3 Conclusions

In summary, this study presents the first systematic characterization and analysis of incineration products from waste flexible perovskite modules, providing comprehensive insights into material transformations and dynamic compositional evolution during thermal decomposition. Our findings demonstrate that controlled incineration, when accompanied by rigorous control measures for harmful gas and toxic substance emissions, represents an environmentally sound and economically viable disposal strategy for waste flexible perovskite modules. These findings are largely extendable to rigid perovskite modules through appropriate process optimization. This investigation not only establishes an empirical foundation for understanding incineration mechanisms in next-generation PV waste, but also proposes practical strategies and fundamental scientific principles to guide industrial-scale recycling of perovskite solar modules.

4 Experimental section

4.1 Materials

PTAA (average M_n 7000–10,000), BCP, PbI_2 (99.999% trace metals), dimethylformamide (DMF), 1-methyl-2-pyrrolidinone (NMP), and toluene were purchased from Sigma-Aldrich and used without further purification. C_{60} was purchased from Nanjing Zhiyan Inc. Formamidinium iodide (FAI), methylammonium chloride (MACl), and cesium iodide (CsI) were purchased from Greatcell. Flexible PET/ITO substrates were purchased from Langu Electronic Technology Co., Ltd.

4.1.1 Module fabrication. The flexible substrates with patterned P1 lines were first UV-ozone treated for 10 minutes before use. The hole-transporting layer, PTAA, with a concentration of 3.3 mg mL^{-1} dissolved in toluene, was blade-coated onto substrates at a speed of 20 mm s^{-1}. The gap between the blade-coater and ITO substrates was 150 μm. Then, a 2.38 M precursor solution of $Cs_{0.1}FA_{0.9}PbI_3$, containing additional 5 mol% PbI_2 and 12.5 mol% MACl, was prepared in a solvent mixture of DMF and NMP at a volume ratio of 5.2 : 1. This solution was subsequently diluted to obtain a final concentration of 1.1 M. The precursor solution was then blade-coated on

the substrates coated with PTAA, utilizing a gap of 300 μm and a movement speed of 20 mm s^{-1}. The nitrogen knife was operated at a pressure of 30 psi and a movement speed of 5 mm s^{-1} after the coating process. Following this, the perovskite films were annealed at 120 °C for 30 minutes in ambient air. C_{60} (30 nm at 0.25 Å s^{-1}), BCP (6 nm at 0.1 Å s^{-1}), and Cu (35 nm at 0.5 Å s^{-1}) were then evaporated onto the perovskite layer sequentially. P2 lines were scribed with a laser marker (345 nm), and then the second layer of Cu was evaporated with a thickness of 130 nm. The flexible modules were completed with P3 line scribed with the same laser marker.

4.1.2 Module incineration and analysis. A flexible module (10 cm × 10 cm) was placed in a chamber, and then subjected to complete incineration in a fume hood assisted with a butane-powered heat gun under continuous air supply. Following the incineration process, the resulting ash was allowed to cool to ambient temperature before being carefully transferred into specimen bottles using a stainless-steel spatula. The collected ash sample was subsequently prepared for compositional analysis and material characterization. The chemical states of elements in the ash obtained from incineration were detected by XPS (Thermo Fisher Scientific K-Alpha). The XPS test used an Al Kα X-ray source and had a spot size of 400 μm. The XRD patterns were acquired with a Bruker D8 ADVANCE X-ray diffractometer. Furthermore, the experiment was conducted using TG-MS for real-time monitoring of the weight loss and formation of gaseous substances. The TG analyzer used was the PerkinElmer TGA 8000, while the mass spectrometer was the PerkinElmer Clarus SQ 8T. In this experiment, a waste flexible module was cut to a piece size of 0.3 cm × 0.3 cm and then placed in a platinum crucible. The sample was heated in ambient air at a 10 °C min^{-1} rate. The mass loss of the sample was recorded continuously as a function of temperature. Simultaneously, the mass spectrometer was used to detect and analyze the volatile compounds released during the heating process. Inductively coupled plasma mass spectrometry (ICP-MS) was performed on an Agilent 7800 instrument.

Author contributions

S. C. conceived the idea for the study and designed the experiments. X. S. fabricated flexible perovskite solar modules, and performed characterization of incineration products. Y. L., T. L. and S. L. assisted with the module fabrication. F. W. assisted with the data analysis of mass spectrometry. X. S. and S. C. wrote the manuscript with inputs from all co-authors. All authors discussed the results and reviewed the manuscript.

Conflicts of interest

The authors declare no competing financial interest.

Data availability

The data supporting this article have been included in this article or as part of the supplementary information (SI). Supplementary information is available. See DOI: https://doi.org/10.1039/d5sc07083j.

Acknowledgements

This work was supported by the National Key Research and Development Program of China (No. 2023YFB3809700), National Natural Science Foundation of China (No. 52372196), and the open research fund of Suzhou Laboratory (SZLAB-1308-2024-TS007).

Notes and references

1 X. Xiao, N. Xu, X. Tian, T. Zhang, B. Wang, X. Wang, Y. Xian, C. Lu, X. Ou, Y. Yan, L. Sun, F. You and F. Gao, *Nature*, 2025, **638**, 670–675.
2 N. Kannan and D. Vakeesan, *Renewable Sustainable Energy Rev.*, 2016, **62**, 1092–1105.
3 H. H. Pourasl, R. V. Barenji and V. M. Khojastehnezhad, *Energy Rep.*, 2023, **10**, 3474–3493.
4 D. Sah, Chitra and S. Kumar, *Sol. Energy Mater. Sol. Cells*, 2022, **246**, 111908.
5 M. S. J.-P. Correa-Baena, T. Buonassisi, M. Grätzel, A. Abate, W. Tress and A. Hagfeldt, *Science*, 2017, **358**, 739–744.
6 Y. Rong, Y. Hu, A. Mei, H. Tan, M. I. Saidaminov, S. I. Seok, M. D. McGehee, E. H. Sargent and H. Han, *Science*, 2018, **361**, 1214.
7 R. Deng, N. L. Chang, Z. Ouyang and C. M. Chong, *Renewable Sustainable Energy Rev.*, 2019, **109**, 532–550.
8 R. Vinayagamoorthi, P. B. Bhargav, N. Ahmed, C. Balaji, K. Aravinth, A. Krishnan, R. Govindaraj and P. Ramasamy, *J. Environ. Chem. Eng.*, 2024, **12**, 111715.
9 D. Sah and S. Kumar, *Sol. Energy*, 2024, **273**, 112534.
10 Y. Xu, J. Li, Q. Tan, A. L. Peters and C. Yang, *Waste Manage.*, 2018, **75**, 450–458.
11 S. Verma, T. Lee, E. Sahle-Demessie, M. Ateia and M. N. Nadagouda, *Chem. Eng. J. Adv.*, 2023, **13**, 100421.
12 J.-K. Lee, J.-S. Lee, Y.-S. Ahn, G.-H. Kang, H.-E. Song, J.-I. Lee, M.-G. Kang and C.-H. Cho, *Sol. Energy Mater. Sol. Cells*, 2017, **160**, 301–306.
13 V. Savvilotidou, A. Antoniou and E. Gidarakos, *Waste Manage.*, 2017, **59**, 394–402.
14 P.-H. Chen, W.-S. Chen, C.-H. Lee and J.-Y. Wu, *Sustainability*, 2023, **16**, 60.
15 M. Tao, V. Fthenakis, B. Ebin, B. M. Steenari, E. Butler, P. Sinha, R. Corkish, K. Wambach and E. S. Simon, *Prog. Photovoltaics Res. Appl.*, 2020, **28**, 1077–1088.
16 J. Tao and S. Yu, *Sol. Energy Mater. Sol. Cells*, 2015, **141**, 108–124.
17 F. Ardente, C. E. L. Latunussa and G. A. Blengini, *Waste Manage.*, 2019, **91**, 156–167.
18 P. R. Dias, L. Schmidt, N. L. Chang, M. Monteiro Lunardi, R. Deng, B. Trigger, L. Bonan Gomes, R. Egan and H. Veit, *Renewable Sustainable Energy Rev.*, 2022, **169**, 112900.
19 G. A. Heath, T. J. Silverman, M. Kempe, M. Deceglie, D. Ravikumar, T. Remo, H. Cui, P. Sinha, C. Libby,

S. Shaw, K. Komoto, K. Wambach, E. Butler, T. Barnes and A. Wade, *Nat. Energy*, 2020, **5**, 502–510.
20 T. Abzieher, D. T. Moore, M. Roß, S. Albrecht, J. Silvia, H. Tan, Q. Jeangros, C. Ballif, M. T. Hoerantner, B.-S. Kim, H. J. Bolink, P. Pistor, J. C. Goldschmidt, Y.-H. Chiang, S. D. Stranks, J. Borchert, M. D. McGehee, M. Morales-Masis, J. B. Patel, A. Bruno and U. W. Paetzold, *Energy Environ. Sci.*, 2024, **17**, 1645–1663.
21 L. Duan, D. Walter, N. Chang, J. Bullock, D. Kang, S. P. Phang, K. Weber, T. White, D. Macdonald, K. Catchpole and H. Shen, *Nat. Rev. Mater.*, 2023, **8**, 261–281.
22 M. Tammaro, J. Rimauro, V. Fiandra and A. Salluzzo, *Renewable Energy*, 2015, **81**, 103–112.
23 M. Akhter, A. Al Mansur, M. I. Islam, M. S. H. Lipu, T. F. Karim, M. G. M. Abdolrasol and T. A. H. Alghamdi, *Sustainability*, 2024, **16**, 5785.
24 S. Chen, Y. Deng, H. Gu, S. Xu, S. Wang, Z. Yu, V. Blum and J. Huang, *Nat. Energy*, 2020, **5**, 1003–1011.
25 H. E. Al-Hazmi, G. K. Hassan, T. A. Kurniawan, B. Śniatała, T. M. Joseph, J. Majtacz, G. Piechota, X. Li, F. A. El-Gohary, M. R. Saeb and J. Mąkinia, *J. Environ. Manage.*, 2024, **354**, 120414.
26 X. Yu, Q. Sui, S. Lyu, W. Zhao, X. Cao, J. Wang and G. Yu, *Environ. Int.*, 2020, **135**, 105404.
27 H. I. Abdel-Shafy, A. M. Ibrahim, A. M. Al-Sulaiman and R. A. Okasha, *Ain Shams Eng. J.*, 2024, **15**, 102293.
28 R. Kumar, A. Verma, A. Shome, R. Sinha, S. Sinha, P. K. Jha, R. Kumar, P. Kumar, Shubham, S. Das, P. Sharma and P. V. Vara Prasad, *Sustainability*, 2021, **13**, 9963.
29 D. Cudjoe and H. Wang, *Fuel Process. Technol.*, 2022, **237**, 107470.
30 X. Zhang and B. Liu, *Sustainability*, 2024, **16**, 3579.
31 X. Wang, J. Li, R. Guo, X. Yin, R. Luo, D. Guo, K. Ji, L. Dai, H. Liang, X. Jia, J. Chen, Z. Jia, Z. Shi, S. Liu, Y. Wang, Q. Zhou, T. Wang, G. Pan, P. Müller-Buschbaum, S. D. Stranks and Y. Hou, *Nat. Photonics*, 2024, **18**, 1269–1275.
32 J. Chen, X. Wang, T. Wang, J. Li, H. Y. Chia, H. Liang, S. Xi, S. Liu, X. Guo, R. Guo, Z. Jia, X. Yin, Q. Zhou, Y. Wang, Z. Shi, H. Zhou, D. Lai, M. Zhang, Z. Xing, W. R. Leow, W. Yan and Y. Hou, *Nat. Energy*, 2024, **10**, 181–190.
33 G. Wang, D. Xu, J. Tang, B. Liu, Z. Wang, Q. Xu, Y. Hu, J. Zhou and S. Wang, *Combust. Flame*, 2023, **255**, 112909.
34 G. Guo, K. Fan, Z. Guo and W. Guo, *Energy*, 2023, **280**, 128202.
35 J. Tang, L. Liu, Z. Yu, J. Du, X. Cai, M. Zhang, M. Zhao, L. Bai, Z. Gai, S. Cui, X. Li and T. Jiu, *Adv. Sustainable Syst.*, 2022, **6**, 2100510.
36 S. Rades, F. Oswald, S. Narbey, J. Radnik and V. D. Hodoroaba, *Surf. Interface Anal.*, 2018, **50**, 1234–1238.
37 C. Das, M. Wussler, T. Hellmann, T. Mayer and W. Jaegermann, *Phys. Chem. Chem. Phys.*, 2018, **20**, 17180–17187.
38 W. Li, J. Fan, J. Li, Y. Mai and L. Wang, *J. Am. Chem. Soc.*, 2015, **137**, 10399–10405.
39 J. Zhang, S. Cao, L. Gong, H. He, Z. Fang, C. Zhou and J. Chen, *Mater. Sci. Semicond. Process.*, 2023, **163**, 107564.
40 X. Jiang, K. Dong, P. Li, L. Zheng, B. Zhang, Y. Yin, G. Yang, L. Wang, M. Wang, S. Li, L. Zhu, S. Niu, S. Yu, S. Liu, W. Tian, X. Guo, M. Wei, S. M. Zakeeruddin, L. Sun, S. Pang and M. Grätzel, *Angew. Chem., Int. Ed.*, 2024, **64**, e202414128.
41 C. Nunes de Carvalho, A. M. Botelho do Rego, A. Amaral, P. Brogueira and G. Lavareda, *Surf. Coat. Technol.*, 2000, **124**, 70–75.
42 S. Lædre, L. Mendizabal, O. E. Kongstein, A. Oedegaard, H. Karoliussen and F. Seland, *J. Electrochem. Soc.*, 2022, **169**, 034504.
43 Y. Li, G. Zhao, X. Zhi and T. Zhu, *Surf. Interface Anal.*, 2007, **39**, 756–760.
44 Y. Li, J. Zhao, J. Han and X. He, *Mater. Res. Bull.*, 2005, **40**, 981–989.
45 J. Yang, M. Huang, S. Wang, X. Mao, Y. Hu and X. Chen, *Water*, 2020, **12**, 3583.
46 L. A. Carvalho, J. D. Ardisson, R. M. Lago, M. D. Vargas and M. H. Araujo, *RSC Adv.*, 2015, **5**, 97248–97255.
47 M. Zhong, J. Li, L. Zhou, T. Wang, J. Liu, M. Mei and S. Chen, *J. Anal. Appl. Pyrolysis*, 2023, **172**, 106002.
48 Z. Wu, X. Cai and Z. Yang, *J. Nanopart. Res.*, 2015, **17**, 329.
49 H. Gaspar, L. Fernandes, P. Pereira and G. Bernardo, *Polym. Bull.*, 2015, **72**, 1775–1786.
50 S. Aghili, M. Panjepour and M. Ghiaci, *Diamond Relat. Mater.*, 2022, **124**, 108943.
51 A. Tadashi, I. Shoji, N. Hideaki and F. Nobuyuki, *Thermochim. Acta*, 1997, **319**, 139–149.
52 T. Ma, R. Wang, W. Wang, W. Gu, Y. Yuan, A. Zhang and J. Wei, *Polym. Degrad. Stab.*, 2022, **206**, 110185.
53 Z. Sebestyén, E. Barta-Rajnai, J. Bozi, M. Blazsó, E. Jakab, N. Miskolczi and Z. Czégény, *Energy Procedia*, 2017, **105**, 718–723.
54 X. Wang, B. Dong, M. Feng, D.-J. Xue and S.-M. Wang, *J. Mater. Chem. A*, 2022, **10**, 15861–15864.